Available online at www.sciencedirect.com
SCIENCE DIRECT
ELSEVIER
Polymer 46 (2005) 1982–1994
polymer
www.elsevier.com/locate/polymer

Comparison of the gelation dynamics for polystyrenes prepared by conventional and living radical polymerizations: a time-resolved dynamic light scattering study

Tomohisa Norisuye[a,*], Takashi Morinaga[b], Qui Tran-Cong-Miyata[a], Atsushi Goto[b], Takeshi Fukuda[b], Mitsuhiro Shibayama[c]

[a]*Department of Polymer Science and Engineering, Kyoto Institute of Technology Matsugasaki, Sakyo-ku, Kyoto 606-8585, Japan*
[b]*Institute for Chemical Research, Kyoto University, Uji, Kyoto 611-0011, Japan*
[c]*Neutron Science Laboratory, Institute for Solid State Physics, The University of Tokyo, Tokai, Naka-gun, 106-1 Shirakata, Ibaraki 319-1106, Japan*

Received 10 August 2004; received in revised form 9 December 2004; accepted 28 December 2004
Available online 18 January 2005

Abstract

The structure and dynamics for the two types of polystyrene gels prepared by conventional and living radical polymerizations have been investigated by time-resolved dynamic light scattering (TRDLS). The reaction was initiated with the monomer solutions with and without a reversible addition–fragmentation chain transfer (RAFT) agent and was monitored through the gelation process. In the absence of a cross-linker, the reaction process was characterized by the appearance of a maximum when the excess scattering intensity divided by concentration was plotted as a function of reaction time. The intensity maximum was ascribed to an increase in the molecular weight and subsequent suppression of the concentration fluctuations, which was qualitatively reproduced by the Flory–Huggins free energy formula. As the concentration became higher, the time–intensity correlation functions (ICFs) exhibited two modes, suggesting the formation of larger aggregates in addition to the cooperative mode. The intensities were successfully decomposed into the two components by taking account of the relative amplitude of the fast and slow modes. The difference of the time-course between the two types of polymerizations was clearly detected by combining TRDLS and gel permeation chromatography, GPC, data. For the cross-linking system, the kinetics was characterized by the universal gelation mechanism, namely: (1) divergence of the slow mode and (2) appearance of the power law in ICF around the gelation threshold regardless of the polymerization method. On the other hand, the real time intensity decomposition analysis revealed striking differences in the gelation mechanism between the two types of polymerization. For example, the slow mode appeared at an early stage of reaction for the conventional system and sustained its amplitude through the gelation process. For the living (RAFT) system, the appearance of the slow mode was limited in a narrower range of the reaction time with a much smaller amplitude.

Keywords: Gels; Dynamic light scattering; Living radical polymerization

1. Introduction

Cross-linking is a promising route to construct an important class of materials such as smart gels, interpenetrating networks, and polymer hybrids. Owing to the ability to immobilize polymer chains as well as small molecules trapped inside the mesh, polymer gels have versatile applications, such as a catalyst support, fuel cell membranes, molecular sieves and so on [1,2]. In general, there are two ways to prepare gels. One is (A) copolymerization of vinyl and divinyl monomers in the presence of a solvent (monomer cross-linked gels), and the other is (B) introduction of cross-links into a homogeneous solution of long polymers (polymer cross-linked gels). In our previous study [3], we investigated the structural inhomogeneities of the hydrogels prepared by (A) copolymerization and (B) γ-ray irradiation by means of dynamic light scattering (DLS) and small-angle neutron scattering (SANS). The main conclusion drawn in that study is illustrated in Fig. 1

* Corresponding author. Tel.: +81 75 724 7853; fax: +81 75 724 7853.
E-mail address: nori@kit.jp (T. Norisuye).

0032-3861/$ - see front matter © 2005 Elsevier Ltd. All rights reserved.
doi:10.1016/j.polymer.2004.12.043

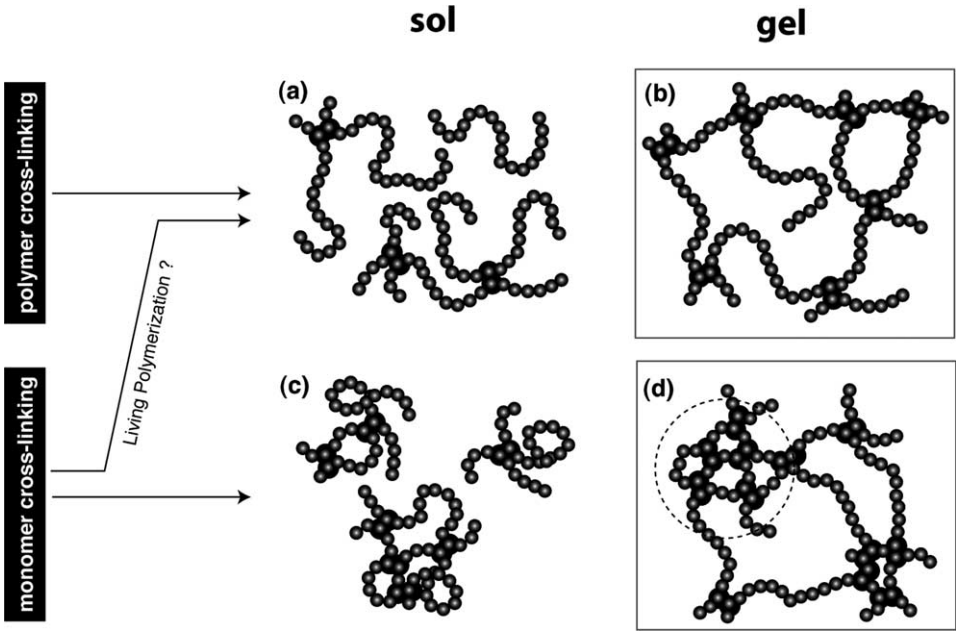

Fig. 1. Schematic representation of the polymer networks prepared by the polymer cross-linking (top) and monomer cross-linking (bottom) methods.

where the upper (a,b) and lower (c,d) parts indicate systems (A) and (B), respectively. These techniques allowed us to observe the hierarchal structure of the gels by detecting the local concentration fluctuations [4,5]. Since concentration fluctuations are 'frozen in' during the course of gelation, the obtained gels have inherent inhomogeneities irrespective of the cross-linking methods. However, the monomer cross-linked gels were more heterogeneous than the γ-ray cross-linked gels because of the additional inhomogeneities induced by the formation of intramolecularly cross-linked clusters [6–8]. Since copolymerization is a convenient way to prepare gels, and since the homogeneities of the gels on the length scale of transport pass have important effect on sieving, permeation and transport properties, it is highly desirable to somehow eliminate those inhomogeneities from the gels.

In recent years, living radical polymerization (LRP) has proved to be a powerful method to synthesize low-polydispersity polymers [9–22]. The variants of LRP include nitroxide-mediated polymerization [13–15], atom transfer radical polymerization [16–19] and reversible addition–fragmentation chain transfer (RAFT) polymerization [20]. The basic mechanism of LRP common to all the variants is a reversible activation process (Scheme 1(a)). Namely, the dormant species P–X is activated to the alkyl radical P$^{\cdot}$ by thermal, photochemical, and/or chemical stimuli with a rate constant k_{act} which, in the presence of monomer M propagates until it is deactivated to P–X, where k_{deact} and k_p are the rate constants for deactivation and propagation, respectively. A number of activation/deactivation cycles provide the chains with an almost equal probability to grow, thus producing low-polydispersity polymers. The activation process of RAFT polymerization includes: (1) the addition of the propagating radical to the dormant species to form the intermediate radical and (2) the subsequent fragmentation of the intermediate radical into another propagating radical and dormant species, as shown in Scheme 1(b).

The aim of this study is to explore the possibility to construct a more homogeneous network by the monomer cross-linking method in conjunction with RAFT process. Owing to the living nature of the RAFT mediated polymerization, the reaction process is characterized by a slow and simultaneous growth of chains with a constant number of primary chains throughout the course of polymerization and gelation. This would lead to fairly random distribution of cross-links for the RAFT system compared to the conventional radical polymerization system, as suggested in previous work [8,23]. In this study, we deal with a well-known system consisting of styrene (St) and divinylbenzene (DVB) for studying

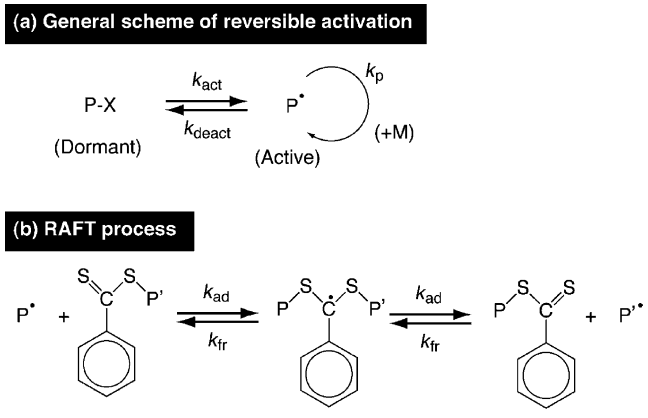

Scheme 1. Reversible activation processes.

vitrification as well as gelation in bulk, which will simplify the interpretation of the results.

2. Experimental section

2.1. Samples

Reagent grade styrene (St) and azobis-isobutyronitrile (AIBN) were obtained from Nakalai Tesque, Japan. St was purified by a standard method including reduced-pressure distillation, while AIBN was recrystallized from methanol. The RAFT agent cumyl dithiobenzoate (CDB) and *p*-divinylbenzene (*p*-DVB) were prepared according to the methods reported by Moad et al. [24] and Storey [25], respectively. Tetrabromomethane, CBr_4, was obtained from Wako Pure Chemical, Japan, and used as received.

For linear polymerization systems, prescribed amounts of AIBN and the RAFT agent were mixed in St and charged in an optically purified glass cell. After degassing and filtration through a 0.2 μm pore size filter, the solution was heated for various periods of time at 60 °C. The sample characteristics are summarized in Table 1, where [St], [A] and $M_{p,calc}$ denote the molar concentrations of St and the chain transfer agent (CBr_4 or CDB) and the expected number-average molecular weight of the primary chain at full conversion, respectively. Here we studied three systems of different RAFT concentrations, which are coded $R200_L$, $R400_L$ and $R800_L$ with $M_{p,calc}=2\times10^4$, 4×10^4 and 8×10^4, respectively. In the absence of any chain transfer agent (Control), the number-average molecular weight of the primary chain at full conversion reaches 15×10^4. The conventional polymerization system coded $C200_L$ includes the chain transfer agent CBr_4 to lower the $M_{p,calc}$ to the level of $R200_L$ so that the two systems can be compared without significant effects of chain length difference.

For cross-linking polymerization systems, AIBN, RAFT and DVB were mixed in St followed by the similar preparation procedure to the linear polymerization. Sample codes with subscript C are abbreviated names for cross-linking system.

2.2. Measurements

Time-resolved dynamic light scattering (TRDLS) measurements were conducted on a DLS/SLS-5000 compact goniometer (ALV, Langen, Germany) coupled with a 22 mW helium–neon laser source (Uniphase, USA). A high counting rate of scattered intensity and a high coherence (more than 0.98) in intensity correlation function (ICF) were achieved by use of a set of static and dynamic enhancers and a high-quantum efficient avalanche-photo diode detection system. The TRDLS measurements were carried out at 60 °C as a function of polymerization time, t. ICF was calculated in a wide range of logarithmic lag time, $\log \tau$, at a fixed angle of 90°.

Gel permeation chromatographic (GPC) analysis was carried out at 40 °C on a Tosoh GPC-8020 high-speed liquid chromatography system equipped with a guard column (Shodex GPC KF-G) and two columns (Shodex GPC KF-804L). Tetrahydrofuran (THF) was used as an eluent at a flow rate of 0.8 ml/min. The column system was calibrated with Tosoh standard PSts. A known amount of sample solution (of a known concentration) was injected in the column system, and the elution profile was analyzed with a Tosoh differential refractometer RI-8020 calibrated with known concentrations of PSts in THF.

Table 1
Polymerization conditions

(a) Linear polymerization

Sample code	$C200_L$	$R200_L$	$R400_L$	$R800_L$
[St]	8.38 M			
Transfer agent	CBr_4	CDB (RAFT)	CDB (RAFT)	CDB (RAFT)
[A]	30.8 mM	41.8 mM	20.9 mM	10.5 mM
[A]/[St]	1/200	1/200	1/400	1/800
Initiator	AIBN (53.5 mM)			
$M_{p,calc}$	2×10^4	2×10^4	4×10^4	8×10^4

(b) Cross-linking polymerization

Sample code	$Cont_C$	$C200_C$	$R200_C$	$R400_C$
[St]	8.38 M			
Transfer agent	None	CBr_4	CDB (RAFT)	CDB (RAFT)
[A]	None	30.8 mM	41.8 mM	20.9 mM
[A]/[St]	None	1/200	1/200	1/400
[DVB]	400 mM			
Initiator	AIBN (26.6 mM)			
$M_{p,calc}$	NA	2×10^4	2×10^4	4×10^4

3. DLS analysis [26]

3.1. Linear polymerization systems

The time averaged intensity, $\langle I(t)\rangle_T$, and its ICF, $g_T^{(2)}(t)$, expressed by

$$g_T^{(2)}(t) \equiv \frac{\langle I(0)I(t)\rangle_T}{\langle I(0)\rangle_T^2} = 1 + |g^{(1)}(t)|^2 \quad (1)$$

are obtained by DLS, where $\langle\cdots\rangle_T$ denotes time average. $\langle g^{(1)}\rangle_T$ is the scattering field time-correlation function given by

$$g^{(1)}(t) = \int G(\tau)\exp(-t/\tau)\mathrm{d}\tau \quad (2)$$

where τ is the relaxation time, and $G(\tau)$ is the characteristic decay time distribution function. For semi-dilute and concentrated polymer solutions, two relaxation modes [27–29] corresponding to mutual diffusion and viscoelastic relaxation [30–32] or large-scale heterogeneities [33] have been reported in the literature. The fast mode was also often referred to as cooperative or collective diffusion. This relaxation behavior strongly depends on solvent quality, molecular weight, scattering angle and so on. The following equation may be applicable to fit the experimental data by taking into account the fact that the slow mode has long time-tail distribution,

$$g_T^{(2)}(q,t) - 1 = \sigma_I^2[A_f \exp(-t/\tau_f) + A_s \exp\{-(t/\tau_s)^\beta\}]^2 \quad (3)$$

Here, τ_f is the fast relaxation time, σ_I^2 is the initial amplitude of the intensity correlation function. The arithmetic relaxation time, $\langle\tau_s\rangle$, can be calculated by integrating $g^{(1)}(t)$ with Eqs. (2) and (3) as,

$$\langle\tau_s\rangle = \int \exp\{-(t/\tau_s)^\beta\}\mathrm{d}t = \frac{\tau_s}{\beta}\Gamma\left(\frac{1}{\beta}\right) \quad (4)$$

where $\Gamma(x)$ is the gamma function of x. A non-linear least-squares fit analysis to Eq. (3) gives relaxation time and its amplitude, which will be presented as a function of the reaction time or conversion. Several hundreds of the intensity and ICF data were systematically analyzed by a homemade software. With a set of A_f, A_s, and σ_I^2 data, the total intensity will be decomposed into the intensity components for the fast, slow and solvent contributions by

$$I_{fast} = \langle I\rangle_T A_{fast}\sqrt{\sigma_I^2} \quad (5)$$

$$I_{slow} = \langle I\rangle_T(1 - A_{fast})\sqrt{\sigma_I^2} \quad (6)$$

$$I_{solvent} = \langle I\rangle_T - I_{fast} - I_{slow} = \langle I\rangle_T\left[1 - \sqrt{\sigma_I^2}\right] \quad (7)$$

where $I_{solvent}$ is the intensity component for unreacted (and/or oligomeric) styrene, which acts as a solvent in the reaction process. Because of the extremely fast motion of the solvent, we do not observe the time correlation in the target time range (10^{-3}–10^4 ms) but it has an important contribution to the intensity [34–36].

3.2. Cross-linking polymerization systems

Provided that ICFs can be represented by a model function, the relaxation time and its amplitude can be determined by the curve fitting procedure as stated above. However, none of the model functions could sufficiently describe the ICF for the cross-linking system. Therefore, we alternatively performed CONTIN [37,38] analysis and estimated parameters by evaluating each intensity component [39]. The proportional constant of regularizer (strength of regularization) and the grid points were set to be 0.5 and 150, respectively. The intensity components for the fast and slow modes will be calculated by integrating intensity components of $G(\tau)$ as

$$I_{fast} = \langle I\rangle_T \sum_{i\in fast} G_i(\tau_i) \quad (8)$$

$$I_{slow} = \langle I\rangle_T \sum_{i\in slow} G_i(\tau_i) \quad (9)$$

$$I_{solvent} = \langle I\rangle_T - I_{fast} - I_{slow} = \langle I\rangle_T\left[1 - \sqrt{\sigma_I^2}\right] \quad (10)$$

while the arithmetic averages of the relaxation times for the fast and slow modes will be given by

$$\tau_{fast} = \sum_{i\in fast} \tau_i G_i(\tau_i) \quad (11)$$

$$\tau_{slow} = \sum_{i\in slow} \tau_i G_i(\tau_i) \quad (12)$$

4. Results and discussion

4.1. Linear polymerization systems

Fig. 2 represents the number-average molecular weight, M_n, and the number of molecules per unit volume, N, as a function of conversion, c. The figure clearly indicates the difference in the polymerization process between the RAFT ($R200_L$, $R400_L$, $R800_L$) and conventional radical polymerization systems ($C200_L$). For example, M_n for the RAFT system linearly increased with c while that for the conventional system rapidly increased in the beginning of the reaction followed by a nearly constant value independent of c. On the other hand, N is almost constant for the RAFT system, while it linearly increases with c for the conventional system. The polydispersity indices, M_w/M_n, for $R200_L$ and $C200_L$ are 1.10 and 1.70 for $c=0.1$,

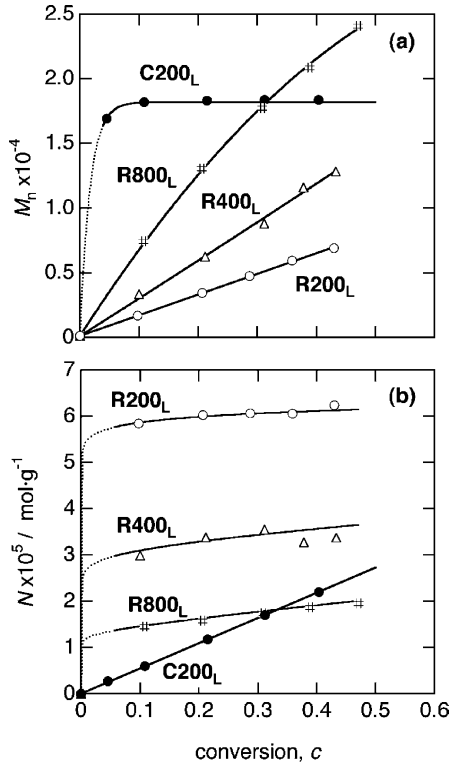

Fig. 2. (a) Number-average molecular weight, M_n, and (b) number of molecules per unit volume, N, estimated by GPC.

respectively. For the conventional system, an initiated radical undergoes propagation to be a high polymer and termination with another propagating radical. This occurs typically in a second. Subsequently, new chains are born and terminated, thus resulting in a linear increasing of N with c.

Fig. 3 shows the c dependence of the reduced excess scattering intensity, $\Delta I/c \equiv \{\langle I\rangle_T - \langle I\rangle_{T,0}\}/c$, where $\langle I\rangle_{T,0}$ is the initial intensity or the intensity of the system with $c=0$. For all the samples, the $\Delta I/c$ vs. c curve is characterized by a peak in a small c region (region I) and a subsequent gradual increase of $\Delta I/c$ with increasing c (region II). In region I, the

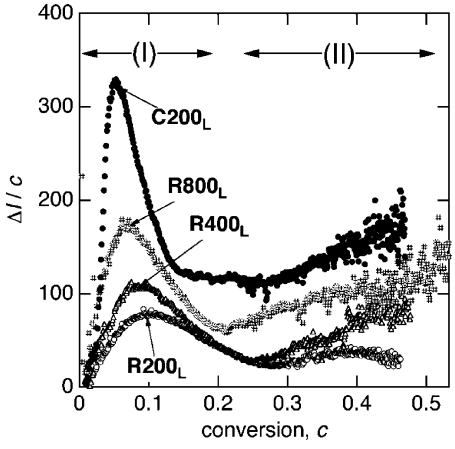

Fig. 3. $\Delta I/c$ as a function of c for $R200_L$, $R400_L$, $R800_L$ and $C200_L$.

increase of $\Delta I/c$ may be attributed to the increase in the molecular weight. The decrease of $\Delta I/c$ after going through the maximum at $c \cong 0.1$ may be due to suppression of the concentration fluctuation.

Let us discuss the origin of the peak found in region (I). First, we estimated the overlap concentration [40] expressed by,

$$c^* = \frac{3M_w}{4\pi N_A \langle S^2\rangle_z^{3/2}} \tag{13}$$

where M_w and $\langle S^2\rangle_z^{1/2}$ are the weight-averaged molecular weight and the z-average radius of gyration, respectively. $\langle S^2\rangle$ can be calculated by,

$$\langle S^2\rangle = \frac{aL}{3} - a^2 + \frac{2a^3}{L}\left[1 - \frac{a}{L}\left\{1 - \exp\left(-\frac{L}{a}\right)\right\}\right] \tag{14}$$

with

$$L = M/M_L = M/390 \tag{15}$$

according to the model proposed by Kratky and Porod [41]. The persistence length a for PSt in the bulk was set to be $a=$ 1.0 (nm) [42], which gave $c^* \cong 0.10$, 0.31, 0.43 and 0.77 for $C200_L$, $R800_L$, $R400_L$ and $R200_L$, respectively. The experimentally observed peak position for $C200_L$ is comparable with the calculated c^*, while those for the RAFT systems, all close to $c \cong 0.1$, are quite different from the calculated values of c^*. Therefore, the concept of intensity suppression by chain overlap cannot be considered to be the main reason for the appearance of the peak.

Next, we tried to calculate the intensity based on the fluctuation theory proposed by Einstein [43] and Smoluchowski [44], where we employed the Flory–Huggins formula [45] of Gibbs free energy to simplify the discussion. According to the theory, the osmotic pressure, Π, is given by

$$\Pi = -\frac{k_B T}{V_0}\left[\log(1-\phi_1) + \phi_1\left(1 - \frac{1}{n}\right) + \chi\phi_1^2\right] \tag{16}$$

where k_BT, V_0, ϕ_1, n and χ are the Boltzmann energy, the molar volume of solvent, the volume fraction of polymer, the degree of polymerization (DP) and Flory's interaction parameter, respectively. Because the reciprocal reduced intensity is proportional to the osmotic modulus,

$$\frac{K\phi_1}{\Delta I} = \frac{\partial(\Pi/N_A k_B T)}{\partial\phi_1} \tag{17}$$

where K and N_A are the optical constant for light scattering and Avogadro's number, respectively. By substituting Eq. (16) into Eq. (17), one gets,

$$\frac{\Delta I}{\phi_1} = 1/\left[\frac{1 + (n-1)\phi_1}{n\phi_1(1-\phi_1)} - 2\chi\right]\phi_1 \tag{18}$$

When the left-hand-side of Eq. (18) is plotted against ϕ_1, the curve exhibits a peak depending on n and χ.

Fig. 4(a) shows the plot of $\Delta I/c$ vs. c calculated with

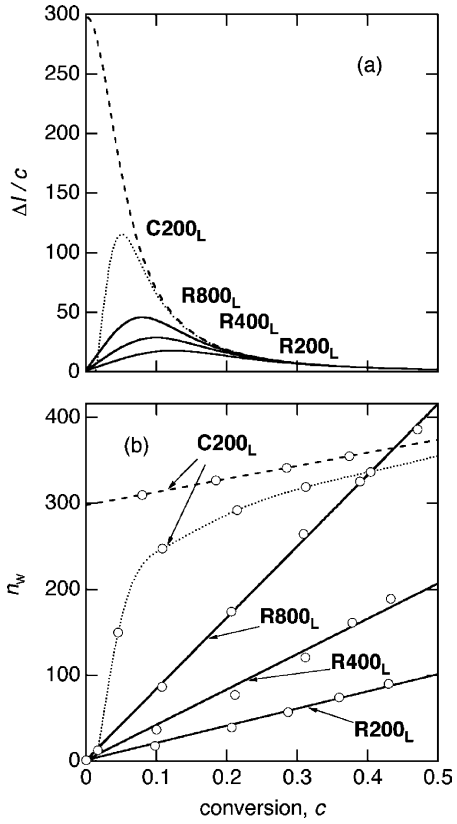

Fig. 4. Variations of (a) $\Delta I/c$ calculated by Eq. (18) and (b) the weight-average DP, n_w, obtained by GPC as a function of c for $R200_L$, $R400_L$, $R800_L$ (solid lines) and $C200_L$ (broken and dotted lines: see text).

Eq. (18), where the weight-averaged degree of polymerization, n_w, obtained by GPC was used for the calculation. χ was set equal to 0.5, for the result is not strongly dependent on χ. As indicated by the solid lines, good agreement between experimental data and calculated intensities was found for the RAFT systems ($R200_L$, $R400_L$ and $R800_L$). While n_w linearly increased with c for the RAFT system, that for the conventional system, $C200_L$, exhibited a larger constant value throughout the reaction process, as indicated by the dashed line in Fig. 4(b). The $\Delta I/c$ vs. c curve calculated with this n_w for $C200_L$ did not exhibit a peak (the dashed line in Fig. 4(a)). Then we reexamined the GPC curves for this system to find low-mass species, which are not usually observed in conventional radical polymerization without a chain transfer agent. These low-mass species, ca. $M_n = 780$ with a fraction of 2%, may be tentatively ascribed to the characteristic of CBr_4 system known as telomerization [46]. With those low-mass components taken into account, the peak for $C200_L$ was successfully reproduced as shown by the dotted line. Note that Eq. (18) predicts the scattering intensity behavior at $q = 0$, i.e., the thermodynamic limit. However, since the scattering vector employed for the DLS experiments is much smaller than the reciprocal of the size of polymer chains, resulting in an invariance of $\Delta I/c$ with respect to q in this q range. Hence, the variation of $\Delta I/c$ with respect to reaction time can be discussed with Eq. (18).

Next, we carried out the intensity decomposition analysis by combining both static and dynamic light scattering methods in order to account for the increase in $\Delta I/c$ for the higher c (region II, Fig. 3). In the beginning of the reaction, where PSt chains were in dilute regime, ICF exhibited a rather monotonic decay, as shown in Fig. 5. As the concentration becomes higher, ICF exhibits two modes, suggesting the evolution of PSt chains and existence of larger length scale fluctuations. The origin of these modes for polymeric systems has been discussed in a large number of references [27–33]. When we enter the semi-dilute regime, where chains overlap with each other, the interpretation of the dynamics becomes complicated by the complex forms of osmotic pressure, friction coefficient, ζ, and the diffusion equation characterized by the coupling between diffusion and stress. Einaga and co-workers studied the effect of viscoelastic relaxation and carried out the decoupling between the relaxation and the diffusion for polyisobutylene and polystyrene solutions in various solvents [32,47]. The fast mode is due to the mutual diffusion of polymer and solvent molecules, while the slow mode is mainly ascribed to the viscoelastic relaxation of entangled polymer chains as discussed by Adam et al. [27] and Stepanek et al. [29]. The amplitude of the fast mode strongly depends on solvent quality. For example, a single decay without the slow mode is observed for PSt in benzene, a good solvent. On the other hand, the amplitudes of both modes are comparable in cyclohexane, a theta solvent. This is due to the fact that the osmotic modulus of solutions is dominated by the fast mode, which results in strong dependence on solvent quality. In our case, a single decay was observed in the early stage of the reaction, whereas the amplitude of the slow mode increased with the evolution of the longer polymer chains. This means that the solvent quality varies from a good to a theta solvent condition, in good agreement with the classical notion of the similarity of the bulk polymer environment and the theta condition [45].

Even though these papers mainly focused on the topological entanglement, the slow modes presented in Fig. 5 seem to bear a different physical origin because the molecular weight of the PSt is not sufficiently larger for chain entanglement and/or overlapping. As a matter of fact, separate experiments (not shown here) have confirmed that these modes are diffusive, namely, the decay rate is proportional to the square of the wave vector. This behavior may be ascribed to the stacking of phenyl groups. However, investigation of the structure of such aggregates is beyond the scope of this work, and we proceed to evaluate the intensity components from time evolution of ICF. As indicated by solid lines in Fig. 5, ICFs were well described by the double exponential function in Eq. (3). By a systematic fitting analysis of the series of ICF data, we obtained the relative amplitude and the relaxation time as a function of time.

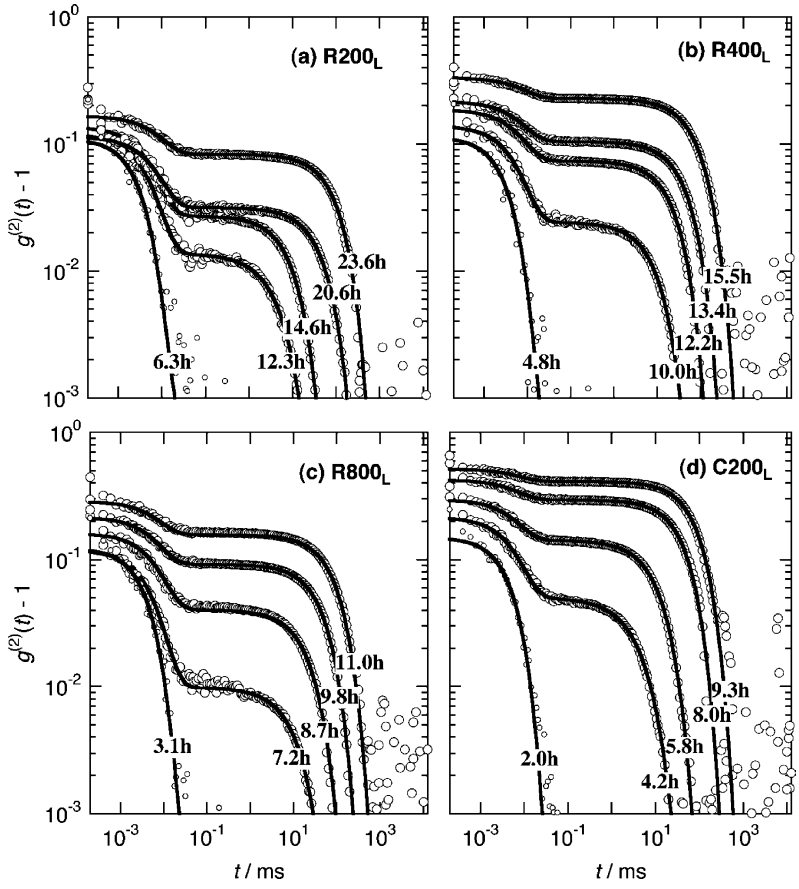

Fig. 5. Reaction time dependence of $g_T^{(2)}(t)$ for (a) $R200_L$, (b) $R400_L$, (c) $R800_L$ and (d) $C200_L$. The solid lines indicate the curve fitting results with Eq. (3).

As shown in Fig. 6, the scattering intensity was successfully decomposed into the fast, slow and solvent contributions for all the systems. As a consequence of the decomposition analysis, the increase of intensity in the high c region (region II, Fig. 3) can be ascribed to the contribution from the slow mode. Note that the solvent mode has a larger contribution in the early stage of the reaction followed by a gradual decrease of intensity with increasing conversion.

In order to confirm the reproducibility of the decomposed intensities, we have carried out measurements with another batches. As shown in Fig. 7, the intensity decomposition was successful for the three individual experiments. The upper and lower parts of the figures represent the results for $C200_L$ and $R200_L$, respectively. Here, the intensity component for the fast mode, I_{fast}, was completely compatible with others, while that for the slow mode, I_{slow}, was different from run to run for $C200_L$. On the other hand, the behavior of I_{slow} for $R200_L$ strongly depended on each run. With increasing M and c, the mobility of the chains would decrease. Since the M for $R200_L$ is much smaller than that for $C200_L$, stacking of phenyl groups [48] may be easier for $R200_L$ than for $C200_L$. In addition, I_{slow} for $C200_L$ was always an increasing function owing to its lower mobility, whereas that for $R200_L$ may probe various scattering volumes due to slow movements of the domains inside the test tube with a certain freedom of the mobility. After the reaction, PSt became glassy, leading to the position dependent strong scattering called speckles, where the large-scale heterogeneities dominate the static structure factor.

4.2. Cross-linking polymerization systems

Similar to the linear polymerization systems, the ICFs of the PSt/DVB cross-linking systems exhibited a monotonic decay at the initial stage of the reaction, followed by the appearance of the slow mode, as shown in Fig. 8. We attempted to fit the data to model functions, such as a double exponential function and a power law function, to find no satisfactory result for describing the gelation process. We then carried out the CONTIN analysis and evaluated the relative amplitudes by integrating the corresponding intensity components. Fig. 8 represents the variation of ICF during gelation. The slow mode shifted to a longer relaxation time as the cross-linking reaction proceeded, and the gelation threshold was determined by the appearance of power law behavior and the longest relaxation time. The threshold was estimated to be 3.20 h, 46.9 min, 14.8 h and 7.75 h for $C200_C$, $Cont_C$, $R200_C$ and $R400_C$, respectively.

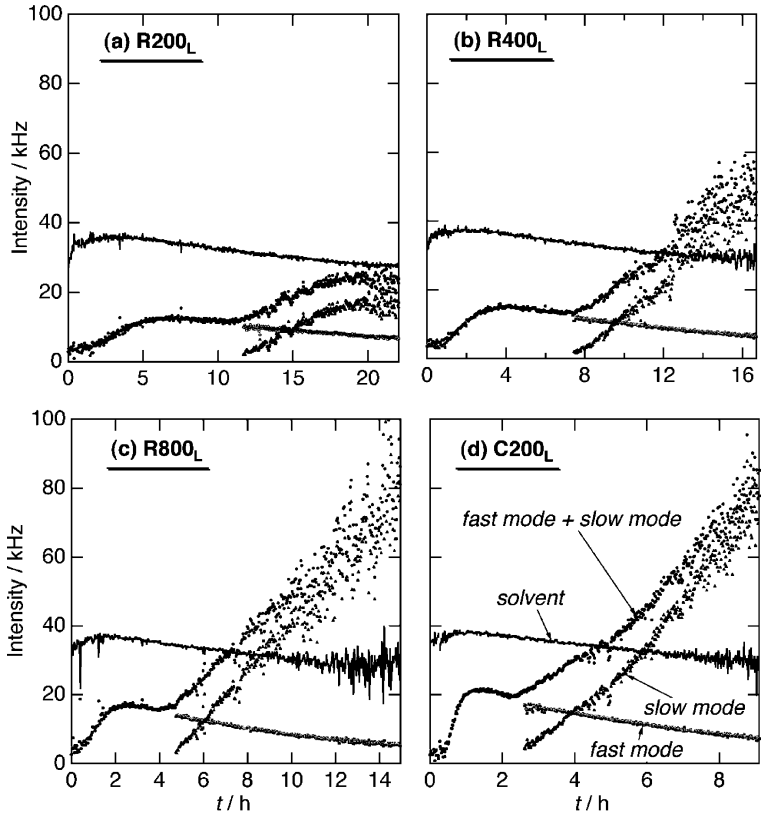

Fig. 6. The intensity components of the fast, slow and, solvent modes decomposed by Eqs. (5)–(7) for (a) $R200_L$, (b) $R400_L$, (c) $R800_L$ and (c) $C200_L$.

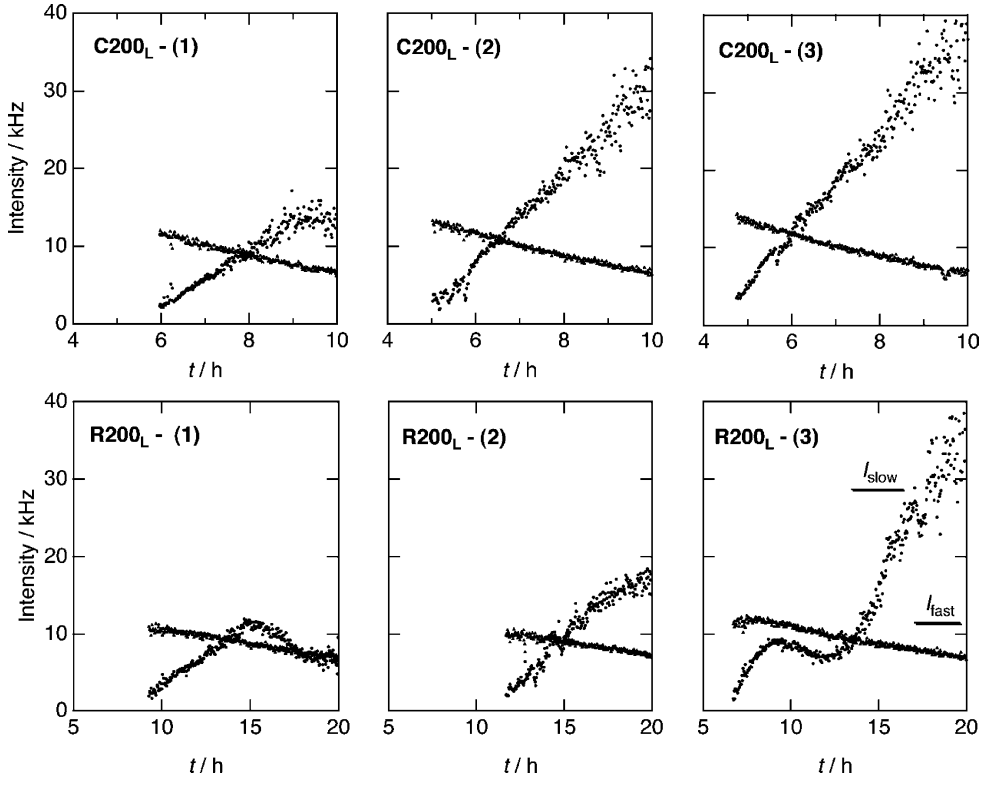

Fig. 7. Reproducibility of the time-course of the intensities for $C200_L$ (top) and $R200_L$ (bottom).

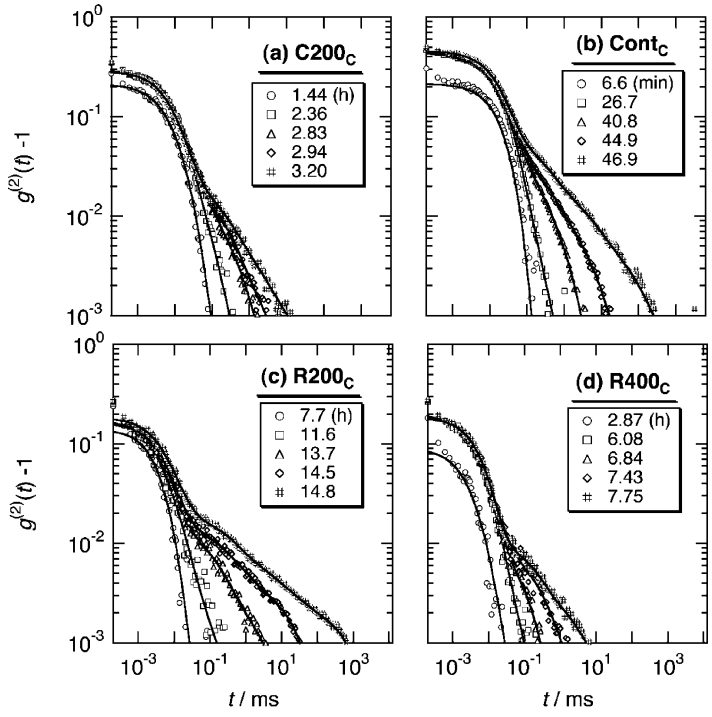

Fig. 8. Reaction time dependence of $g_T^{(2)}(t)$ for (a) $C200_C$, (b) $Cont_C$, (c) $R200_C$ and (d) $R400_C$. The solid lines indicate the curve fitting results with CONTIN software.

The solid lines indicate the results reproduced by the CONTIN analysis. It is well known that the ICF becomes a power law function around gelation threshold, which is expressed by

$$g_T^{(2)}(q,t) - 1 = \sigma_I^2[A_f \exp(-t/\tau_f) + A_s(1 + t/t^*)^{(\alpha-1)/2}]^2 \quad (19)$$

Here α and t^* are the critical exponent and the lower cutoff, respectively, of the power law behavior. This equation is known to well reproduce the experimental data around the gelation threshold for various gelling systems. While the theoretical treatment has been in controversy, the relation between α and the network structure has been extensively discussed elsewhere [49]. The value of α was evaluated as 0.54, 0.55, 0.70 and 0.56 for $C200_C$, $Cont_C$, $R200_C$ and $R400_C$, respectively.

Since the fitting was quite successful, quantitative evaluation of the intensity components was subsequently carried out. The results of intensity decomposition analysis were exhibited in Fig. 9. In spite of an ill-posed problem [37] for inverse Laplace transformation, the fast, the slow and the solvent modes were successfully evaluated as a function of reduced reaction time, t/t_{gel}, where t_{gel} is the gel time. As described in the previous section, an induction period was observed for $C200_C$ system. On the other hand, the intensity increased immediately after the reaction had been initiated for $Cont_C$. For $R200_C$ and $R400_C$, the intensity was rather low and more gradually increased. Note that the time-course of cross-linking process was quite reproducible, which was in strong contrast with the linear polymerization system (Fig. 7). This may be ascribed to the compactness of the clusters, leading to less entanglement and stacking of phenyl groups.

The reaction time dependence of I_{fast} and I_{slow} is summarized in Fig. 10(a) and (b), respectively, where solid squares, solid diamonds, open circles and open triangles indicate $C200_C$, $Cont_C$, $R200_C$ and $R400_C$, respectively. As seen in Fig. 10(a), I_{fast}s for the conventional system ($C200_C$ and $Cont_C$) increased more drastically than that for the RAFT system. The drastic increase in I_{fast} for the conventional systems is probably due to formation of large molecules emerged from a very early stage of the reaction. We have observed a significant contribution of the slow mode not only for the conventional systems but also for the RAFT systems (Fig. 10(b)). However, I_{slow}s for $R200_C$ and $R400_C$ are much smaller than those for $C200_C$ and $Cont_C$. More interestingly, I_{slow} appeared in the middle stage of the reaction for the conventional systems, whereas it appeared near the gelation threshold for the RAFT systems, suggesting the formation of a more homogenous gel in the latter.

Fig. 11 exhibits reaction time dependence of τ_{fast} and τ_{slow} for (a) $C200_C$, (b) $Cont_C$, (c) $R200_C$ and (d) $R400_C$ calculated with Eqs. (11) and (12). τ_{fast} is a weak function of t/t_{gel}. On the other hand, τ_{slow} for all the systems clearly diverged around gelation threshold, i.e., $t/t_{gel} = 1$, suggesting the divergence of the relaxation time is a universal phenomenon for gelling systems. Here, the value of τ_{fast} at the late state of the reaction contains interesting

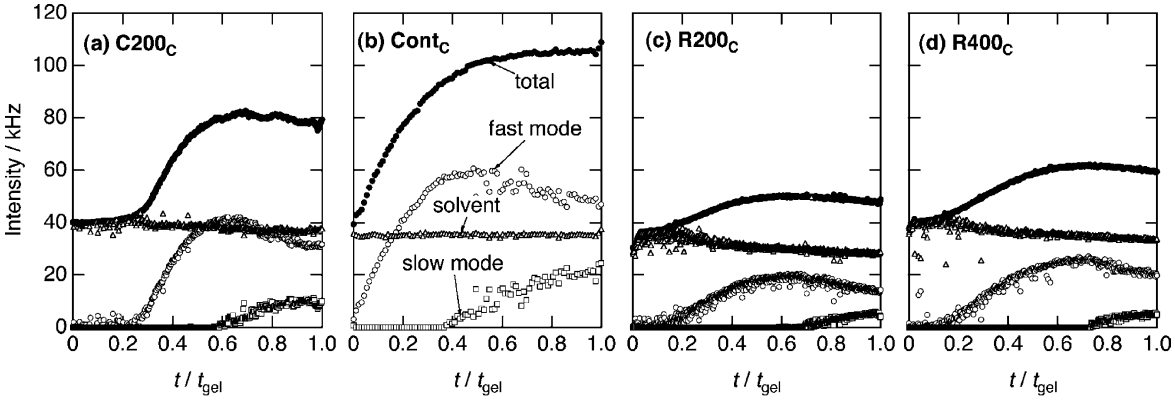

Fig. 9. The intensity components of the fast, slow and solvent modes decomposed by Eqs. (8)–(10) for (a) $C200_C$, (b) $Cont_C$, (c) $R200_C$ and (d) $R400_C$.

information about the difference between the conventional and RAFT systems. For example, if the dynamics is dominated by heterodyne contribution due to inhomogeneous gelation for the conventional system, τ_{fast} will be larger (theoretically twice of that for the homodyne mode), as indicated by Fig. 11.

Finally, we wish to stress difference in gelation process and gel structure between the conventional and RAFT systems. In the conventional system, (dead) polymers of full length are formed from an early stage of reaction. Since polymers in dilute solution seldom find other polymers nearby, cross-links will be formed mostly within the same molecule (intra-chain cross-linking), as previously evidenced by the shrinkage of chains by this cause [50]. As the reaction proceeds, and the number of such chains increases, inter-chain cross-linking will also occur, combining chains into larger molecules. Once large molecules are formed, they will absorb other chains more effectively to produce large heterogeneities in solution, which, in the final stage, will be tied up into a huge molecule filling the whole space, i.e., the gelation. In this picture [8], the gel from the conventional system is highly heterogeneous. In the RAFT system, on the other hand, the number concentration of primary chains is high and constant from the beginning to the end of reaction, so that cross-links will be introduced more randomly to produce a more homogenous gel than the conventional system [8] (Fig. 12). These pictures are supported by the time-courses of the scattering intensities of the fast and slow components of the two systems (Fig. 10) and are consistent with the previous studies [8,23]. The late stage of reaction may be characterized by a universal gelation behavior irrespective of the reaction methods. In fact, all the samples exhibited the divergence of τ_{slow} and the power law behavior in ICF (Fig. 11). Nevertheless, the fine structure inside the gels must be largely different between the two systems, as already suggested. This will be an interesting topic to study by position-dependent static/dynamic light scattering.

5. Conclusions

The structure and dynamics for two types of polystyrene solutions and gels prepared by conventional and RAFT-mediated living radical polymerizations have been investigated in terms of static/dynamic light scattering (SLS/DLS) and gel permeation chromatography (GPC). Relative amplitudes of the time intensity correlation functions for

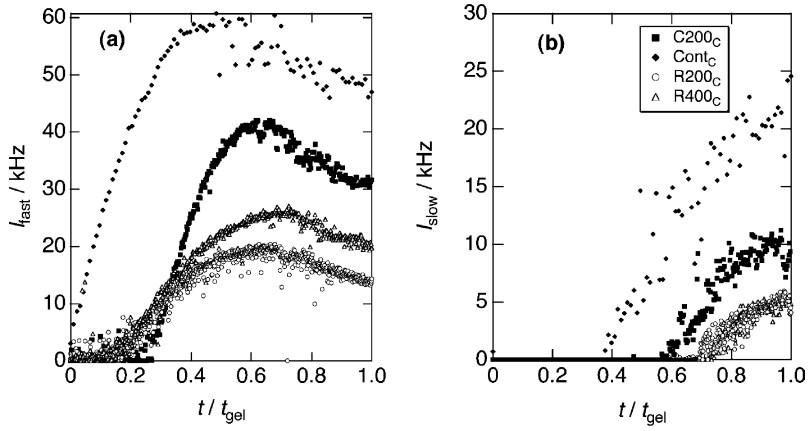

Fig. 10. (a) I_{fast} and (b) I_{slow} as a function of t/t_{gel} for $C200_C$, $Cont_C$, $R200_C$ and $R400_C$.

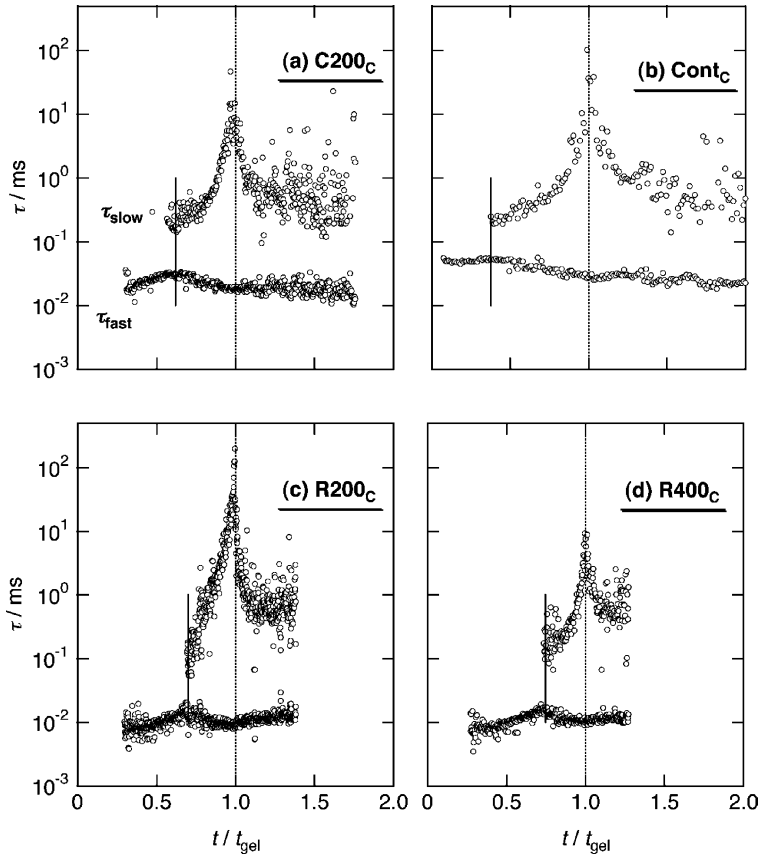

Fig. 11. Fast and slow relaxation times, τ_{fast} and τ_{slow}, as a function of t/t_{gel} for (a) $C200_C$, (b) $Cont_C$, (c) $R200_C$ and (d) $R400_C$.

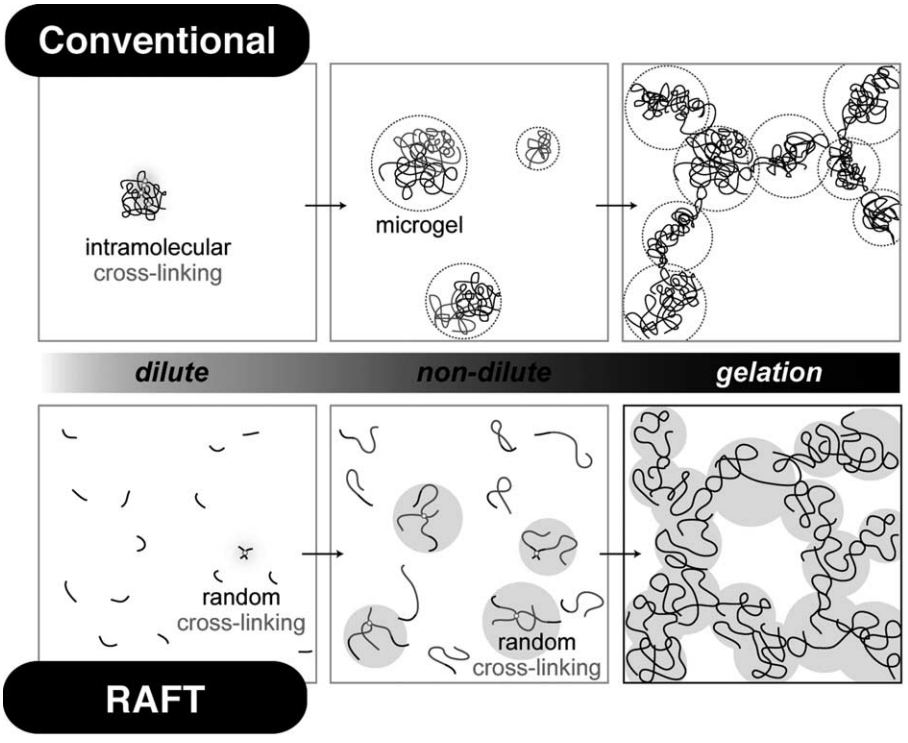

Fig. 12. Schematic representations of the cross-linking process for conventional (top) and living (bottom) radical polymerizations.

the multiple decay components were evaluated by performing the double exponential analysis or the inverse-Laplace analysis using CONTIN package. The total intensities were decomposed into the fast (I_{fast}), slow (I_{slow}) and solvent ($I_{solvent}$) contributions, where I_{fast} and I_{slow} correspond to the cooperative diffusion in semi-dilute solution and the translational diffusion of large aggregates, respectively.

For the linear polymerization systems (without the cross-linker), the scattering intensity exhibited a peak at a characteristic conversion, c, followed by an increase in a high-c region. Appearance of the peak in the initial stage of the reaction was interpreted in terms of the increase in molecular weight and the subsequent suppression of concentration fluctuations. This behavior was qualitatively explained by Flory–Huggins free energy theory. As for the increase of intensity at high c, I_{slow} played an important role in total intensity variation. The slow relaxation was ascribed to the translational diffusion of aggregates, because the decay rate was proportional to the square of wave vector, for one thing, and the molecular weight was much lower than that required for chain entanglement, for another.

For the cross-linking polymerization systems, the scattering intensities were also decomposed into I_{fast}, I_{slow}, and $I_{solvent}$. The I_{fast} for the RAFT system increased more gradually than that for the conventional system. Furthermore, the I_{slow} for the RAFT system was much lower than that for the conventional system and appeared only in a late stage of the reaction. Excepting for this clear difference between the conventional and RAFT polymerizations, the divergence of the relaxation time for the slow mode and the power law behavior in ICF were common to both gelling systems.

These experimental findings would lead to the following pictures of gelation of the two systems: In the conventional system, cyclization or intramolecular cross-linking dominates the early stage of reaction, which introduces large heterogeneities to the solution and the gel. In the RAFT system, where the concentration of primary chains is sufficiently high and constant, the cross-linking reaction occurs more randomly, resulting in a more homogeneous solution and gel. Nevertheless, the gelation would occur in the universal way characterized by the divergence of cluster size and its distribution. We did observe the gelation by detecting the stepwise cluster evolution on the order of several hundreds to several tens of micrometers by means of SLS/DLS technique, irrespective of the synthetic methods of gel formation.

Acknowledgements

This work is supported by Grant-in-Aid, No. 13750832 from the Ministry of Education, Science, Sports, Culture, and Technology.

References

[1] Rossi D, Kajiwara K, Osada Y, Yamauchi A, editors. Polymer gels. New York: Plenum; 1991.
[2] Osada Y, Kajiwara K, editors. Gel handbook. New York: Academic Press; 2001.
[3] Norisuye T, Kida Y, Masui N, Tran-Cong-Miyata Q, Maekawa Y, Yoshida M, Shibayama M. Macromolecules 2003;36:6202.
[4] Higgins JS, Benoit HC. Polymers and neutron scattering. Oxford: Clarendon Press; 1994.
[5] Geissler E. In: Brown W, editor. Dynamic light scattering, the methods and applications. Oxford, England: Oxford University; 1993.
[6] Naghash HJ, Okay O. J Appl Polym Sci 1996;60:971.
[7] Patras G, Qiao GG, Solomon DH. Macromolecules 2001;34:6369.
[8] Ide N, Fukuda T. Macromolecules 1999;32:95.
[9] Matyjaszewski K. Controlled radical polymerization. vol. 658 1998.
[10] Matyjaszewski K. Controlled/living radical polymerization. vol. 768 2000.
[11] Matyjaszewski K. Advances in controlled/living radical polymerization. vol. 854 2003.
[12] Matyjaszewski K, Davis TP. Handbook of radical polymerization. New York: Wiley; 2002.
[13] Solomon DH, Rizzardo E, Cacioli P. Eur. Pat. Appl. EP135280; 1985.
[14] Georges MK, Veregin RPN, Kazmaier PM, Hamer GK. Macromolecules 1993;26:2987.
[15] Hawker CJ, Bosman AW, Harth E. Chem Rev 2001;101:3661.
[16] Kato M, Kamigaito M, Sawamoto M, Higashimura T. Macromolecules 1995;28:1721.
[17] Wang J, Matyjaszewski K. J Am Chem Soc 1995;117:5614.
[18] Kamigaito M, Ando T, Sawamoto M. Chem Rev 2001;101:3689.
[19] Matyjaszewski K, Xia J. Chem Rev 2001;101:2921.
[20] Chiefari J, Chong YK, Ercole F, Krstina J, Jeffery J, Le TPT, Mayadunne RTA, Meijs GF, Moad CL, Rizzardo GME, Thang SH. Macromolecules 1998;31:5559.
[21] Fischer H. Chem Rev 2001;101:3581.
[22] Goto A, Fukuda T. Prog Polym Sci 2004;29:329.
[23] Ide N, Fukuda T. Macromolecules 1997;30:4268.
[24] Le TPT, Moad G, Rizzardo E, Thang SH. International Pat. Appl. PCT/US97/12540 W0981478, Invs.; Chem Abstr. 1998;128:115390.
[25] Storey BT. J Polym Sci Part A: Polym Chem 1965;3:265.
[26] Berne BJ, Pecora R. Dynamic light scattering with applications to chemistry, biology and physics. Mineola, NY: Dover Publications; 2000.
[27] Adam M, Delsanti M, Munch JP, Durand D. Phys Rev Lett 1988;61:706.
[28] Brochard F, de Gennes PG. Macromolecules 1977;10:1157.
[29] Stepanek P. Macromolecules 1998;31:1889.
[30] Doi M, Onuki A. J Phys II France 1992;2:1631.
[31] Einaga Y, Karube D. Polymer 1999;157.
[32] Einaga Y, Fujisawa T. Polymer 2002;43:5105.
[33] Heckmeier M, Mix M, Strobl G. Macromolecules 1997;30:4454.
[34] Norisuye T, Tran-Cong-Miyata Q, Shibayama M. Macromolecules 2004;37:2944.
[35] Joosten JGH, Gelade ETF, Pusey PN. Phys Rev A 1990;42:2161.
[36] Rouf-George C, Munch JP, Schosseler F, Pouchelon A, Beinert G, Boué F, Bastide J. Macromolecules 1997;30:8344.
[37] Provencher SW. Comp Phys Commun 1982;27:213.
[38] Provencher SW, Stepanek P. Part Part Syst Charact 1996;13:291.
[39] Kanao M, Matsuda Y, Sato T. Macromolecules 2003;36:2093.
[40] de Gennes PG. Scaling concepts in polymer physics. Ithaca: Cornell University; 1979.
[41] Kratky O, Porod G. Recl Trav Chim Pays-Bas 1949;68:1106.
[42] Wignall GD, Ballard DGH, Schelten J. Eur Polym J 1973;10:861.
[43] Einstein A. In: Alexander J, editor. Colliod chemistry, vol. 1. New York: Reinhold; 1926, p. 323.
[44] Smoluchowski M. Ann Phys 1908;25:205.

[45] Flory PJ. Principles in polymer chemistry. Ithaca: Cornell University; 1953.
[46] Gleixner G, Breitenbach JW, Olaj OF. Macromol Chem Phys 1977; 178:2249.
[47] Einaga Y, Itaya A. Polymer 2002;4869.
[48] Mao S-Z, Feng H-Q. Colloid Polym Sci 1998;276:247.
[49] Shibayama M, Norisuye T. Bull Chem Soc Jpn 2002;75:641.
[50] Ide N, Tsujii Y, Fukuda T, Miyamoto T. Macromolecules 1996;29: 3851.